ACS Catalysis

Research Article

pubs.acs.org/acscatalysis

# Nanosized Coordination Cages Incorporating Multiple Cu(I) Reactive Sites: Host–Guest Modulated Catalytic Activity

Qi-Ting He,[†] Xiang-Ping Li,[†] Lian-Fen Chen,[†] Li Zhang,*[,†] Wei Wang,[‡] and Cheng-Yong Su*[,†]

[†]MOE Laboratory of Bioinorganic and Synthetic Chemistry/KLGHEI of Environment and Energy Chemistry, School of Chemistry and Chemical Engineering, Sun Yat-sen University, Guangzhou 510275, China

[‡]State Key Laboratory of Applied Organic Chemistry, Lanzhou University, Lanzhou 730000, China

Supporting Information

**ABSTRACT:** The intermolecular catalysis toward the oxidation of hydrocarbons has been studied with a series of nanoscale coordination cages $[Cu^{I}_{4}L_{4}]^{4+}$, which are characteristic of the inherent catalytic activity by installing multiple $Cu^{+}$ redox active ions on the cage vertices. The catalytic reactions take place out-cage on the surface active $Cu^{+}$ sites, while the catalytic activity can be modulated in-cage by the guest anions, establishing an unprecedented host–guest regulable catalysis structural model for coordination cages in the sense of supramolecular catalysis. The catalytic behavior and mechanism, reactivity-structure relationship, and recyclable use of the cage catalysts have been thoroughly explored, in an effort to find the way to achieving robust catalysis through careful tuning of the solution stability and redox activity of cage structures by changing size and shape of guest anions.

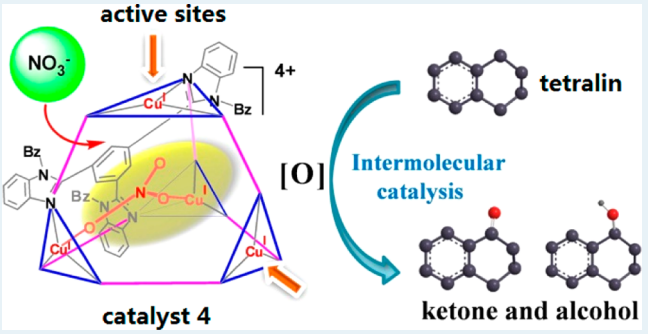


**KEYWORDS:** *cage compounds, copper, host–guest system, C–H activation, supramolecular catalysis*

## 1. INTRODUCTION

The convergent and modular self-assembly of coordination cages with well-defined shape and size can not only provide versatile metalated containers promising for storage, recognition, and delivery applications, but also offer a platform for supramolecular catalysis to mimic the pocket nature of enzymes.[1−9] On one hand, the cages structures are inherent in shape- and size-confined cavity to enable catalytic selectivity and specificity; on the other hand, the cage complexes are characteristic of multiple metal and organic sites that are anchored onto the nanoscale sphere to endow catalytic heterogeneity and multifunctionality.[10−12]

So far, most coordination cages are reported to behave as molecular flasks,[1] limiting their catalytic behaviors merely to cage cavity, either by accelerating reactions through the proximity effect and preorganization of substrates into reactive conformations or by accomplishing reactions via encapsulation of reactive metal motifs.[13−17] Assembly of self-supported catalytic coordination cages incorporating active sites or integrating modulation reminiscent of allosteric nature of enzymes remains largely unexplored.[18−22] In this context, the design of redox active coordination cages with robust, host–guest-dependent catalytic activity may feature in (1) installing multiple active sites or functional groups, (2) combining stereochemistry and catalysis characteristics, (3) facilitating either in-cage or out-cage reactions, and (4) allowing supramolecular recognition or modulation.

Copper and silver complexes have played an increasing role in catalysis, especially in the most challenging field of C–H bond activation of hydrocarbons.[23−26] Degradation of metal catalysts in solution is one of the major problems, needing design of a better structural model to increase the turnover of the conventional catalysis. It is our group's long-term interest to develop robust coordination hosts in both the solid state and solution and apply the $Cu^{+}$ and $Ag^{+}$ metal sources of low coordination number and potential active sites to create catalytically active coordination cages.[27−29] If catalytic reactions could be carried out at the metal sites anchored on the cage surface, either in-cage or out-of-cage, such organic soluble cages could not only promote the organic reactions in homogeneous media but also be easy to recycle like heterogeneous catalysts because of their high thermodynamic stability and fast, convergent self-assembly character. Herein, we demonstrate, for the first time, the catalytic potentials of our previously reported $[Cu^{I}_{4}L_{4}]^{4+}$ cages[27] with respect to intermolecular C–H bond activation of hydrocarbons and further clarify the reactivity–structure relationship through fine host–guest modulation of their solution stability and redox activity to explore the way to use these kinds of active $Cu^{+}$ cages as a robust structural model for supramolecular catalysis.

**Received:** September 27, 2012
**Revised:** November 10, 2012
**Published:** November 13, 2012

## 2. EXPERIMENTAL SECTION

**2.1. General Materials and Methods.** All chemicals were of reagent grade obtained from commercial sources and were used without further purification. The C, H, and N elemental analyses were performed on a Perkin-Elmer 240 elemental analyzer. The X-ray powder diffraction was recorded on a Bruker D8 Advance diffractometer at 40 kV, 40 mA with a Cu-target tube and a graphite monochromator. Nuclear magnetic resonance spectra were determined on a Varian Mercury Plus 300 MHz spectrometer instrument. Chemical shifts for $^1$H NMR are reported in parts per million downfield from tetramethylsilane ($\delta$) as the internal standard, and coupling constants are in hertz (Hz). Electrospray ionization mass spectra were performed on a JEOL JMS-T100LP AccuTOF using electrospray ionization (positive ion mode: ESI) in acetonitrile. Infrared spectra were recorded on a Nicolet Avatar 330 FT-IR spectrometer with KBr pellets, and major absorptions are given in cm$^{-1}$. Mass spectra were obtained on an Agilent model 5975C quadrupole mass-selective detector (MSD) that was interfaced with an Agilent model 7890A gas chromatograph (GC). Cuprous nitrate was synthesized from a reaction mixture of $Cu(NO_3)_2{\cdot}3H_2O$ and excess copper foil in acetonitrile, which was refluxed under $N_2$ until the blue solution color was discharged. After 2 h, the reaction mixture was filtered under $N_2$, the filtrate was vacuumed, and a white solid of $CuNO_3$ was obtained and stored under argon for immediate use.

(**Caution!** Perchlorate salts of metal complexes with organic ligands are potential explosives. While we have encountered no incidents in the preparation and reactivity studies of the salts, it is advisable to use only small amounts and to handle the compounds with caution in the presence of wet solvents.)

**2.2. Preparation of Copper Complexes.** The rigid ligand 1,3,5-tris(1-benzylbenzimidazol-2-yl)benzene (L, Figure 1) and Cu(I) complexes $[Cu^I_4L_4]{\cdot}4X$ ($X$ = OTs$^-$, **1**; OTf$^-$, **2**; and $ClO_4^-$, **3**) were synthesized as described in our previous paper.[27]

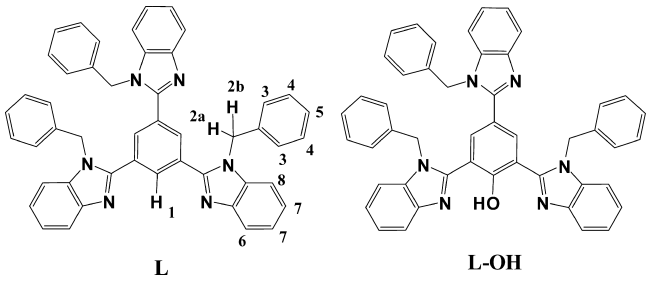


**Figure 1.** Molecular structures of the ligand L and hydroxylated LOH.

Herein, one new Cu(I) complex $[Cu^I_4L_4]{\cdot}4NO_3$ (**4**) was synthesized as follows: To a solution of L (17.4 mg, 0.025 mmol) in 5 mL $CHCl_3$ was added 5 mL of MeOH solution of freshly prepared $CuNO_3$ (6.3 mg, 0.050 mmol). The resulting clear yellow mixture was stirred for 15 min and filtered out, and the clear filtrate was left standing at ambient temperature to evaporate slowly, giving rise to yellow crystals after several days. Yield: 55% based on the ligand. The elemental analysis revealed a formulation of $4{\cdot}4CH_3OH$. Anal. Calcd for $C_{196}H_{160}Cu_4N_{28}O_{16}$: C, 68.88; N, 11.48; H, 4.72. Found: C, 68.34; N, 11.59; H, 4.71%. The phase purity of the bulky sample was checked by PXRD (Supporting Information Figure S1). IR (KBr, cm$^{-1}$, Supporting Information Figure S2) 3431(br), 3084(w), 2914(w), 2520(w), 1797(w), 1604(m), 1528(m), 1452(s), 1412(s), 1383(s), 1350(m), 1329(m), 1282(m), 1161(m), 1076(w), 1028(w), 889(m), 873(m), 754 (m), 725(m), 696(m), 616(w), 553(m), 480(w), 457(w). ESI-TOF-MS (Supporting Information Figure S5): $m/z$ 1034.303 $[Cu^I_4L_4(NO_3)]^{3+}$; 1582.444 $[Cu^I_4L_4(NO_3)_2]^{2+}$. Single crystals suitable for X-ray diffraction analysis were grown under similar conditions, giving a solvent-free structure $\{NO_3^- \subset [Cu^I_4L_4]{\cdot}3NO_3\}$. Single-crystal data: $C_{192}H_{144}Cu_4N_{28}O_{12}$, $M_r$ = 3289.51, orthorhombic, space group $Aba2$, $a$ = 26.5310(4), $b$ = 29.2825(10), $c$ = 21.2848(4) Å, $V$ = 16536.0(7) Å$^3$, $Z$ = 4, $D_{calcd}$ = 1.321 g/cm$^3$, $\mu$ = 1.154 mm$^{-1}$, $T$ = 150(2) K, 8542 observed reflections out of total 11390 with $I > 2\sigma(I)$ ($R_{int}$ = 0.0222), 967 parameters, final $R_1$ = 0.1044, $wR_2$ = 0.2103, CCDC 864852.

Cu(II) complexes $[Cu^{II}_4(LO)_2(H_2O)_2(OTs)_6]$ (**5**) and $[Cu^{II}_2(LH{-}O)_2(OTf)_2](OTf)_2$ (**6**) were prepared as reported previously.[27] A new Cu(II) complex $[Cu^{II}_4(LO)_2(H_2O)_2(NO_3)_6]$ (**7**) was obtained as follows: L (17.4 mg, 0.025 mmol) and $Cu(NO_3)_2{\cdot}3H_2O$ (12.1 mg, 0.050 mmol) were dissolved in 10 mL of MeCN solution. The resulting clear green mixture was transferred to a test tube. The test tube was then sealed in a glass bottle containing 20 mL of diethyl ether. After slow diffusion of the diethyl ether at ambient temperature for a few days, yellow crystals (**4**) appeared. When the sample was kept under the diethyl ether atmosphere for about 1 week, the yellow crystals disappeared, along with growing of more and more green crystals (**7**). Yield: 75% based on the ligand. The elemental analysis of the green crystals revealed a formulation of $7{\cdot}H_2O$. Anal. Calcd for $C_{96}H_{76}Cu_4N_{18}O_{23}$: C, 54.80; N, 11.98; H, 3.64. Found: C, 54.87; N, 11.87; H, 3.67%. IR (KBr, cm$^{-1}$): 3430(s), 2921(w), 1796(w), 1608(w), 1453(m), 1413(m), 1383(s), 1330(m), 1284(m), 1161(w), 1080(w), 1013(w), 874(w), 753(m), 728(m), 697(w), 555(w), 457(w). A differently solvated crystal structure was established by the single-crystal X-ray diffraction from a similar reaction. $7{\cdot}2$MeCN: $C_{100}H_{80}Cu_4N_{20}O_{22}$, $M_r$ = 2168.00, Triclinic, space group $P$-1, $a$ = 13.373(5), $b$ = 13.767(5), $c$ = 14.926(5) Å, $\alpha$ = 104.973(5), $\beta$ = 103.729(5), $\gamma$ = 109.545(5) °, $V$ = 2338.2(14) Å$^3$, $Z$ = 1, $D_{calcd}$ = 1.540 g/cm$^3$, $\mu$ = 1.757 mm$^{-1}$, $T$ = 293(2) K, 4578 observed reflections out of total 7036 with $I > 2\sigma(I)$ ($R_{int}$ = 0.0519), 665 parameters, final $R_1$ = 0.0643, $wR_2$ = 0.1513, CCDC 901630.

**2.3. X-ray Crystallographic Studies.** Experimental details of the X-ray structural analyses as well as the crystallographic data for complexes **4** and **7** are provided in Supporting Information Tables S1 and S3, and selected bond lengths (Å) and angles (°) are listed in Supporting Information Tables S2 and S4, respectively. The diffraction data were collected on an Oxford Gemini S Ultra diffractometer equipped with Cu K$\alpha$ radiation ($\lambda$ = 1.541 78 Å) for complexes **4** (at 150 K) and **7** (at 293 K) by using $\varphi$ and $\omega$ scans. Multi-scan adsorption corrections were applied for the reflections. The structures were solved by the direct methods (SHELXS) and refined by the full matrix least-squares method against $F_0^2$ using the SHELXTL software.[30,31] All the non-hydrogen atoms were refined anisotropically, whereas the hydrogen atoms, except water molecules in **7**, were introduced in calculated positions and refined with fixed geometry with respect to their carrier atoms. In **4**, all $NO_3^-$ anions are disordered and refined with fractional occupancy, and SADI/FLAT or DIFX were applied, which cause 22 restraints. All non-hydrogen atoms were refined with

isotropic simulation by ISOR/SIMU, which gives 828 + 756 restraints. The water molecules in **7** were refined with fixed O−H distance by DFIX, giving rise to 3 restraints.

**2.4. $^1$H NMR Spectroscopic Studies.** $^1$H NMR spectra were recorded on a Varian Mercury Plus 300 MHz spectrometer using an indirect probe. Because of the low solubility of L in $CD_3CN$ and low solubility of cuprous salt in $CDCl_3$, the NMR titration experiments were carried out in a 3:1 (v/v) mixture solution of $CD_3CN/CDCl_3$ at 26 °C. Chemical shifts were referenced to TMS ($\delta$ 0.00), and the $^1$H NMR titration spectra were recorded with the addition of freshly prepared $CuNO_3$ to L dissolved in $CD_3CN/CDCl_3$. First, L ($n_L$ = 2.5 $\mu$mol, 1.7 mg) and $CuNO_3$ ($n_{Cu}$ = 5.0 $\mu$mol, 0.6 mg) were separately dissolved in the mix solvent, giving a 320 $\mu$L and a 200 $\mu$L solution, respectively. Then a quantitative volume solution of $CuNO_3$ was slowly added into the solution of L ($n_L$ = 2.5 $\mu$mol) in five portions successively by microlitre syringe, offering mixtures containing different metal−ligand molar ratios from 1:2 ($\Delta n_{Cu}$ = 1.25 $\mu$mol, 50 $\mu$L) to 1:1 ($\Delta n_{Cu}$ = 1.25 $\mu$mol, 50 $\mu$L), 5:4 ($\Delta n_{Cu}$ = 0.625 $\mu$mol, 25 $\mu$L), 3:2 ($\Delta n_{Cu}$ = 0.625 $\mu$mol, 25 $\mu$L), and 2:1 ($\Delta n_{Cu}$ = 1.25 $\mu$mol, 50 $\mu$L). Each incremental addition was treated in the same NMR tube with heating for 10 min, followed by immediate measurement. In addition, $^1$H NMR spectra of ligand L and complex **4** were determined to compare with those of the in situ titration mixtures, demonstrating the formation process of $[Cu^I_4L_4]^{4+}$ structure in solution. To show the sole structure of $[Cu^I_4L_4]^{4+}$ cage remaining in the solution after catalytic reaction, the reaction mixture was treated by full evaporation under vacuum to yield a residue. This residue was checked by the NMR experiment. Variable temperature $^1$H NMR experiments were carried out over a range of temperatures from 25 to 80 °C in a solution of 400 $\mu$L of $CD_3CN$.

**2.5. Typical Procedure for Catalytic Activity Studies.** Tetralin (0.025 mmol, 3.4 $\mu$L, 1 equiv), $[Cu^I_4L_4]X_4$ cage catalyst (1 mol %), TBHP (*tert*-butyl hydroperoxide, 70% in water, 2.5 $\mu$L, 1 equiv), internal standard naphthalene (3.2 mg, 1 equiv), and 1 mL of MeCN were introduced into a 5 mL flask under ambient atmosphere and stirred at 60 °C, giving a yellow reaction mixture. After refluxing for 24 h, 1.0 $\mu$L of the clear resulting mixture was directly analyzed by GC/MS. The products were confirmed as follows: the MSD was operated in the electron ionization (EI) mode with an ionization potential of 70 eV, a scan range of 10−500 amu, and a normal scan rate of 3.25 scans/s. The GC was fitted with a 30 m × 0.25 mm ID fused-silica capillary column coated with 0.25 $\mu$m 100% PEG, CP9205, VF-WAXms (Varian, Inc.). The oven temperature was programmed as follows: initial temperature, 50 °C; initial hold, 5 min; program rate, 10 °C/min; final temperature, 220 °C; final hold, 10 min. The injector was operated in the split mode (20:1) at 250 °C. The MSD source was operated at 230 °C. Helium was used as the carrier gas.

**2.6. Synthesis of Tetralin-$d_4$ (1,2,3,4-tetrahydronaphthalene-1,1,4,4-$d_4$).** A solution of 2.50 M $NaCD_2SOCD_3$ in $Me_2SO$-$d_6$ was prepared by the method of Corey et al.[32] as follows: sodium hydride (7.5 mmol as a 60% dispersion in mineral oil) in a 25 mL three-necked flask was washed with several portions of hexane to remove the mineral oil. The flask then was equipped with rubber stopples, a reflux condenser fitted with a three-way stopcock, and a magnetic stirrer. The system was alternately evacuated and filled with nitrogen, 3 mL of $Me_2SO$-$d_6$ was introduced via syringe, and the mixture was heated at 80 °C for 3 h. Later, to this solution of $NaCD_2SOCD_3$ in $Me_2SO$-$d_6$ was added tetralin (252 $\mu$L, 1.85 mmol) via syringe, and the mixture was allowed to stir and heated at 80 °C.[33] After 3 days, the reaction was quenched with 150 $\mu$L of $D_2O$, and 10 mL of petroleum ether was then added. The mixture was extracted with two 5 mL portions of $H_2O$. The organic layer was filtered and dried with $MgSO_4$. The solvent was removed under reduced pressure to yield 0.17 g (68%) of crude tetralin with deuterium in the benzylic positions. This procedure was repeated until tetralin-$d_4$ was obtained containing 98.5% D incorporation as judged by GC/MS analysis.

**2.7. Kinetic Isotope Effects (KIEs).** The KIEs for tetralin oxidation were studied by using an equimolar mixture of tetralin (0.0125 mmol, 1.7 $\mu$L, 0.5 equiv) and tetralin-$d_4$ (0.0125 mmol, 1.9 $\mu$L, 0.5 equiv) as substrates (Supporting Information Table S12). The catalyst **4** (1 mol %), TBHP (70% in water, 2.5 $\mu$L, 1 equiv), internal standard naphthalene (3.2 mg, 1 equiv), and 1 mL of MeCN were introduced to a 5 mL flask under ambient atmosphere and stirred at 60 °C, giving a yellow reaction mixture. After 24 h, the reaction mixture was analyzed by GC/MS. The peaks due to possible products 1-tetralone, 1-tetralone-$d_2$ (1-tetralone-4,4-$d_2$), 1-tetralol, and 1-tetralol-$d_3$ (1-tetralol-1,4,4-$d_3$) are well resolved in the GC spectrum under our experiment conditions. Mass spectrum (70 eV): *m*/*z*, 1-tetralone, 146, 131, 118, 90; 1-tetralone-4,4-$d_2$, 148, 133, 120, 92; 1-tetralol, 148, 130, 120, 105, 91; 1-tetralol-1,4,4-$d_3$, 151, 132, 121, 106, 93. The KIE was calculated by the following equation: $k(C_{10}H_{12})/k(C_{10}H_8D_4)$ = (moles of 1-tetralone + 1-tetralol)/(moles of 1-tetralone-4,4-$d_2$ + 1-tetralol-1,4,4-$d_3$).

## 3. RESULTS AND DISCUSSION

**3.1. Design of Structural Model.** Recently, we successfully assembled a series of cuboctahedral $Cu^+$ cages $[Cu^I_4L_4]\cdot 4X$ (X = $OTs^-$, **1**; $OTf^-$, **2**; and $ClO_4^-$, **3**) by using a bulky trigonal ligand 1,3,5-tris(1-benzylbenzimidazol-2-yl)benzene (L) with different $Cu^+$ salts (Scheme 1a).[27] Moreover, such $[Cu^I_4L_4]X_4$ cages can be obtained in an alternative route from reactions of ligand L and $Cu^{2+}$ salts (Scheme 1b) by in situ reduction of $Cu^{2+}$ ions. No matter which copper sources ($Cu^+$ or $Cu^{2+}$) were used, $[Cu^I_4L_4]X_4$ cages were found to crystallize from the mother liquid as the first sole products, which showed thermodynamic stability relying on counteranions and intramolecular hydroxylation, depending on the host−guest adaptability.

**Scheme 1. Synthesis of $Cu^+$ and $Cu^{2+}$ Complexes**

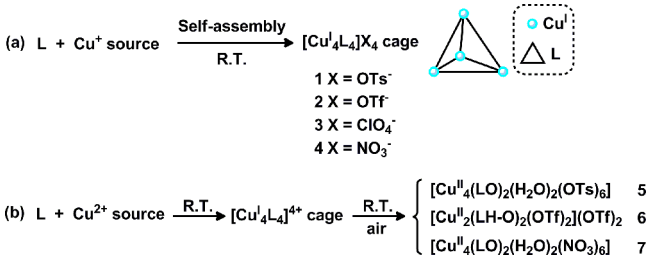


In our previous study, it was found that the small $ClO_4^-$ anion can act as template guest to stabilize the $[Cu^I_4L_4]^{4+}$ cage in solution but significantly blunt redox activity of $Cu^+$ ions, whereas larger $OTs^-$ or $OTf^-$ anions can stay out-cage to keep $Cu^+$ ions highly redox-active but cannot resist rapid self-


dx.doi.org/10.1021/cs300640r | ACS Catal. 2013, 3, 1−9

oxidation of the ligand.[27] Hydroxylation of the ligand (L−OH, Figure 1) under ambient conditions was observed from the structural conversion of the redox-active cages **1** and **2** to $Cu^{2+}$ complexes **5** ($[Cu^{II}_4(LO)_2(OTs)_6(H_2O)_2]$) and **6** ($[Cu^{II}_2(LH{-}O)_2(OTf)_2](OTf)_2$), respectively, when leaving cages **1** and **2** in the mother liquid for several days (Scheme 1b). By contrast, cage **3** is relatively stable, remaining unchanged even when kept in solution for several months. Such host−guest-dependent redox activity and solution stability show promise for these $Cu^+$ cages as supramolecular catalysis structural models for C−H bond oxidation chemistry; however, the problems of intramolecular oxidation (in the cases of cages **1** and **2** with $OTs^-$ and $OTf^-$ anions not acting as proper guests, but destroying the catalysts) and low redox activity (in the case of cage **3**, which is stabilized by a perfect $ClO_4^-$ guest) have to be overcome.

This arouses our interest to make use of such redox-regulable cages as a practical catalyst and accomplish the following challenges: (1) how to maintain solution stability while achieving catalytic robustness toward intermolecular reactivity and (2) how to utilize $Cu^+$ active sites through appropriate host−guest modulation (Scheme 2). A logical approach for

**Scheme 2. Illustration of the Active Sites of $[Cu^I_4L_4]^{4+}$ Cage and Host−Guest Modulated Properties**

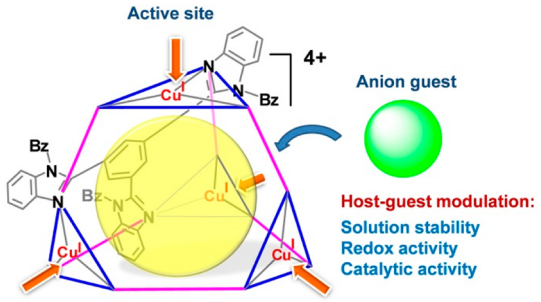


meeting these challenges would be to find an appropriate guest anion that can combine the stability of cage **3** and the activity of cages **1** and **2**. After careful testing selection, we targeted the $[Cu^I_4L_4]^{4+}$ cage using the smaller and planar $NO_3^-$ as the counteranions and found that $NO_3^-$ can template the formation of redox-active cage **4** with enough solution stability while leaving part of the $Cu^+$ sites active for out-cage intermolecular reaction, thus offering favorable heterogeneous supramolecular model balancing solution stability and robust reactivity for homogeneous catalysis.

**3.2. Solution and Solid Structure.** Self-assembly of $CuNO_3$ and ligand L at room temperature readily led to the formation of $\{NO_3^-\subset[Cu^I_4L_4]\cdot 3NO_3\}$ (**4**) cage, which is stable in solution, or even in the presence of bubble oxygen, $H_2O_2$, or TBHP, as long as there are no interfering $Cu^{2+}$ ions. The quantitative formation of cage **4** in solution has been confirmed by $^1$H NMR titration experiments (Figure 2). Upon addition of $CuNO_3$ into the solution of L with metal−ligand molar ratios ranging from 1:2 to 1:1, 5:4, 3:2, and 2:1, the proton signals display remarkable shift, indicative of complexation. At a metal−ligand molar ratio of 1:1, the spectrum converges to one set of well resolved signals, showing two doublet peaks ($\delta$ = 4.05 and 3.44 ppm, $J^2$ = 16 Hz) for $-CH_2-$ protons and remaining unchanged with an excess of $CuNO_3$. The unified proton shifts suggest the formation of the most thermodynamically stable structure in solution, and the methylene peaks'

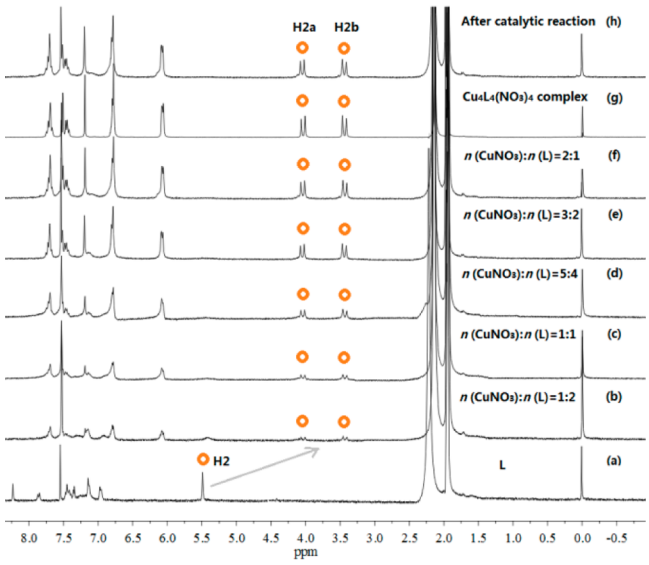


**Figure 2.** The 300 MHz $^1$H NMR spectra ($CD_3CN/CDCl_3$, v/v = 3:1) at 26 °C: (a) L; (b−f) in situ $^1$H NMR titration; (g) cage **4**; (h) catalyst **4** after fourth runs of the oxidation reaction of tetralin.

splitting of geminal protons is characteristic of the $[Cu^I_4L_4]^{4+}$ cage structure (Supporting Information Figure S3).[27] These results prove that cage **4** is thermodynamically stable in solution, even at high temperature (Supporting Information Figure S4), and the dynamic metal−ligand exchange is not detectable in the NMR time scale. Further proof of the solution structure of **4** is obtained by ESI-TOF mass spectral measurement. The ESI-TOF mass spectrum of **4** in MeCN exhibits only the parent $[Cu_4L_4(NO_3)]^{3+}$ ($m/z$ 1034.64) and $[Cu^I_4L_4(NO_3)_2]^{2+}$ ($m/z$ 1582.44) signals, with isotopic distributions exactly matching the simulations (Figure S5), indicative of the sole presence of the $[Cu^I_4L_4]^{4+}$ cage in solution.

In the case of reactions with the $Cu^{2+}$ source (Scheme 1b), the products of $[Cu^I_4L_4]^{4+}$ cages were obtained first, but then disappeared slowly in the presence of excess free $Cu^{2+}$ ions in solution to afford corresponding $Cu^{2+}$ complexes.[27] However, the structural conversion from $Cu^+$ cages to $Cu^{2+}$ complexes is rather different, depending strongly on the nature of the anions. Cages **1** and **2** are much more easily converted to $Cu^{2+}$ complexes **5** and **6**, respectively, along with concomitant hydroxylation of the ligand to phenol compound, but cage **4** is found to transform to $Cu^{2+}$ complex **7** ($[Cu^{II}_4(LO)_2(NO_3)_6(H_2O)_2]$) very slowly. Moreover, the $[Cu^I_4L_4]^{4+}$ cage structure in **4** can be destroyed only in the case that the excess $Cu^{2+}$ ions are present. To confirm this process, we mixed the crystals of **4** with 100 equiv of $Cu^{2+}$ nitrate in $CH_3CN$ for 30 min. The ESI-TOF mass spectral detecting of the mixture showed new peaks of $[Cu^IL]^+$, $[Cu^I_2L(NO_3)]^+$, $[Cu^{II}_2L(NO_3)_3]^+$, and $[Cu^{II}_2L_2(NO_3)_3]^+$, indicating partial dissociation of the $[Cu^I_4L_4]^{4+}$ cage and formation of $Cu^{2+}$ coordination species (Supporting Information Figure S13). After a long standing of cage **4** in solution in the presence of excess $Cu^{2+}$ ions, appearance of green crystals was observed, denoting the final transformation into $Cu^{2+}$ complex **7**. The ESI-TOF mass spectral measurement of the solution also suggested hydroxylation of the ligand, confirmed by observation of peaks assignable to $[LO{-}H]^+$ ($C_{48}H_{36}N_6O$), $[Cu^I_2(LO)]^+$, and $[Cu^I_2L(LO)]^+$ (Supporting Information


dx.doi.org/10.1021/cs300640r | ACS Catal. 2013, 3, 1−9

Figure S13). These results indicate that the $[Cu^{I}_{4}L_4]^{4+}$ cage in **4** with $NO_3^-$ as the anion is more stable in solution than the same $[Cu^{I}_{4}L_4]^{4+}$ cages in **1** and **2** with $OTs^-$ and $OTf^-$ as anions. However, slow structural conversion of cage **4** to $Cu^{2+}$ complex **7** suggests that the $[Cu^{I}_{4}L_4]^{4+}$ cage in **4** still can display redox activity toward catalytic hydroxylation of the ligand.

The X-ray single-crystal analysis unambiguously confirmed the $\{NO_3^-\subset[Cu^{I}_{4}L_4]\cdot 3NO_3\}$ structure of **4**, in which the 2-nm-sized $[Cu^{I}_{4}L_4]^{4+}$ cage is the same as those in **1**–**3** (Figures 3

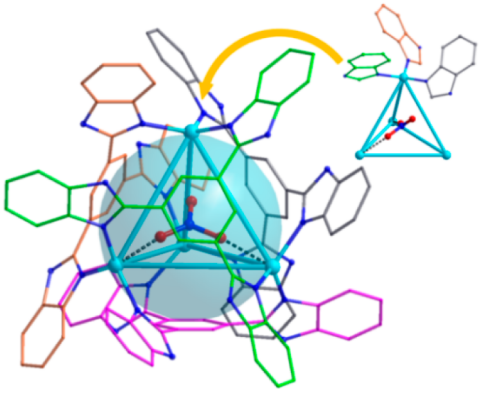

**Figure 3.** Perspective of the $[Cu^{I}_{4}L_4]^{4+}$ cage in **4** with cavity showing in a tetrahedron and host–guest interactions in broken lines. Inset shows the coordination environment of the $Cu^{I}$ vertex, and benzyl groups and H atoms are omitted for clarity.

and S14),[27] except that there is one $NO_3^-$ guest inside the cage and three $NO_3^-$ anions lying outside. Two of the O atoms of the $NO_3^-$ guest interact with two $Cu^+$ ions, forming weak Cu···O bonds (2.325 Å), whereas the third O atom only negligibly interacts with the rest of the $Cu^+$ ions (Cu···O > 2.9 Å). It is worth noting that four $Cu^+$ ions adopt trigonal coordination geometry to occupy the vertex of a tetrahedron with three benzimidazole rings wrapping around in propeller fashion, leaving enough space for small molecules to approach from outside the cage. In contrast, complex **7** shows a tetranuclear structure containing two octahedral and two square–pyramidal $Cu^{2+}$ ions. Each ligand molecule was hydroxylated to $LO^-$ to act as a bridging ligand, chelating two $Cu^{2+}$ ions with the remaining coordination sites occupied by O atoms from $NO_3^-$ anions (Supporting Information Figure S15), which is similar to te previously reported complex **5**.[27]

**3.3. Catalytic Activities of $Cu^+$ Cages.** Oxidation of tetralin is selected as the benchmark reaction to test the catalytic activities of copper coordination cages **1**–**4**. Optimization of the reaction conditions were carried out by selectively evaluating effects of different tetralin-to-**4** molar ratios, oxidant-to-**4** molar ratios, and the amount of solvent used (Supporting Information Table S5–7, Figures S16–18). The results suggest that, on the basis of the tetralin, 1 equiv of TBHP ($^t$BuOOH) and 1 mol % of catalyst are appropriate for all catalytic reactions (see details in Supporting Information). As depicted in Figure 4 and Supporting Information Table S8 (entry 4–7), all four cage complexes can promote the catalytic oxidation of tetralin in MeCN at a mild 60 °C, leading to 1-tetralone and 1-tetralol with preferable selectivity of the carbonyl product. Further optimization experiments gave the conclusion that increased temperature, catalyst, and solvent did not provide better results. However, cage **4** obviously shows

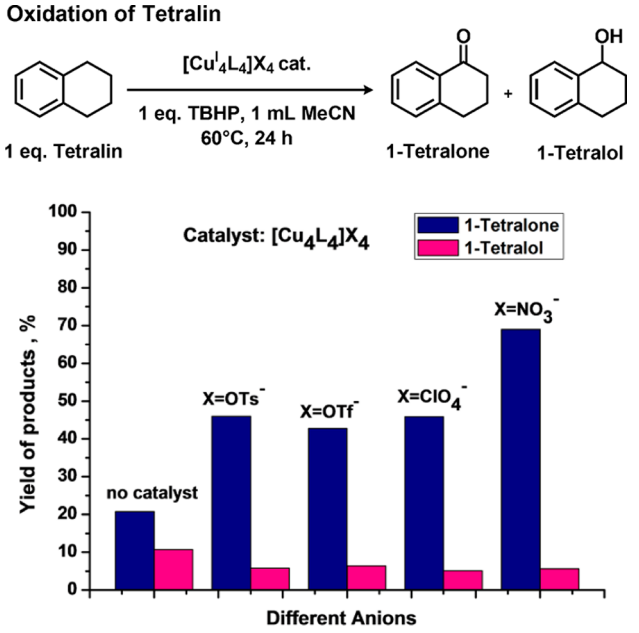


**Figure 4.** Oxidation of tetralin catalyzed by cages **1**–**4**.

superior activity over cages **1**–**3** under the same conditions. Similar results were also observed for oxidation of indane and fluorene (Supporting Information Table S8, entry 8–17). Cage **4** can also catalyze the peroxidative oxidation of acyclic benzyl hydrocarbons, such as ethylbenzene, cumene, and diphenylmethane (Table 1), with moderate yields, but did not work for the oxidation of reluctantly activated cyclohexane.

Since cage structures **1**–**4** differ only in counteranions, the above catalytic results indicate that the host–guest matchup

**Table 1. Products Distribution in the Oxidation of Other Hydrocarbons Catalyzed by 4**[a]

| Entry | Substrate | Yield of products (%)[b] | | Total (%) | Selectivity (%)[c] |
|---|---|---|---|---|---|
| | | Ketone | Alcohol | | |
| 1 | 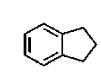 | 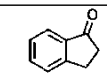 69.8 | 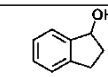 10.8 | 80.6 | 86.6 |
| 2 | 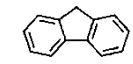 | 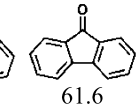 61.6 | N.D. | 61.6 | >99 |
| 3 | 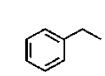 | 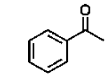 16.8 | 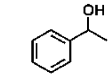 3.6 | 20.4 | 82.4 |
| 4 | 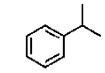 | N.D. | 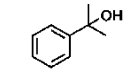 36.0 | 36.0 | >99 |
| 5 | 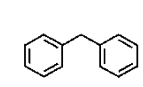 | 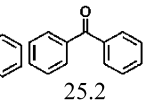 25.2 | 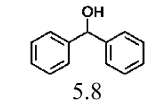 5.8 | 31.0 | 81.3 |
| 6 |  | N.D. | N.D. | - | - |

[a]Reaction conditions: substrate (0.025 mmol, 1 equiv), catalyst **4** (1 mol %), TBHP (70% in $H_2O$, 1 equiv), internal standard naphthalene (1 equiv), MeCN (1 mL), 60 °C, 24 h reaction. Percentage yield and selectivity were determined by GC/MS. [b]Moles of product/100 mol of substrate. [c]Moles of main product/100 mol of (ketone + alcohol).


dx.doi.org/10.1021/cs300640r | ACS Catal. 2013, 3, 1–9

**Scheme 3. Illustration of the Host–Guest Modulation of the Same Coordination Cage Causing Distinctively Different Supramolecular Catalysis**

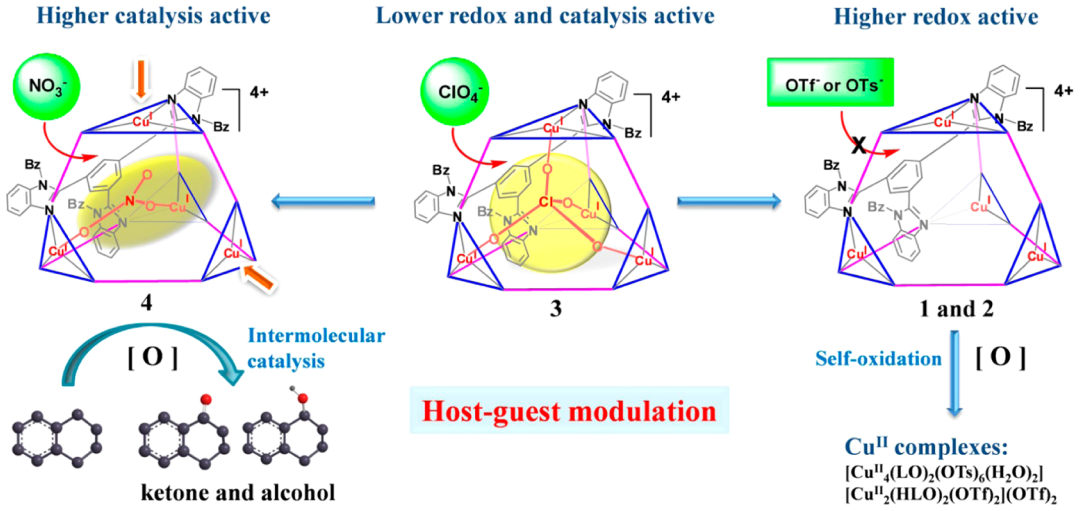


and modulation through cage–anion interactions may play an important role in out-cage intermolecular catalytic activity, which may make contributions from the following aspects: (1) the guest template effect on the thermodynamic and kinetic stability in solution, (2) electrostatic interactions between $Cu^+$ sites and anions dictating redox activity of the cage, and (3) the $Cu^+$ coordination environment determining substrates' access and coordination reorganization during the catalytic process.

As depicted in Scheme 3, the large size of anions in complexes **1** and **2** prevents them from entering the cage, causing relatively low solution stability of cages, which may partially dissociate to establish an equilibrium between $[Cu^I_4L_4]^{4+}$ and segmental species. In contrast, the small size of anions in complexes **3** and **4** are adequate for a template inside the $[Cu^I_4L_4]^{4+}$ cage, giving rise to thermodynamic and kinetic stability of the cages that represent the unique structure in solution against dissociation. These hypotheses have been verified by $^1H$ NMR titration and ESI-TOF MS studies, as shown in Figure 2 and Supporting Information Figures S5–9, laying the primary foundation for choosing solution-stable cages as homogeneous catalysts. Meanwhile, the shape of anions represents another important factor in dictating the cage catalysis. The long $OTs^-$/$OTf^-$ anions in **1** and **2** have to stay outside, leaving four highly redox-active $Cu^+$ corners intact. However, the four out-cage anions may hover over the four $Cu^+$ sites due to the electrostatic attractions, reducing the chances for substrates to approach. The tetrahedral $ClO_4^-$ anion guest in **3** exactly matches the cage cavity, forming weak Cu···O interactions with four $Cu^+$ vertices, thus significantly deactivating the cage redox activity. In contrast, the planar $NO_3^-$ guest in **4** allows only two of O atoms to interact randomly with two of the four $Cu^+$ vertices, leaving the remaining two $Cu^+$ sites free and, thus, still highly active. In addition, it should be noted that, since there remain only three out-cage anions in **3** and **4**, there is always one $Cu^+$ site free of electrostatic interactions with outside anions. This makes the cages **3** and **4** more preferential for out-cage catalysis than **1** and **2**, although in principle, all cages can display out-cage catalytic activity because of their outwardly open $Cu^+$ sites, which are coordination-unsaturated.[34]

On the basis of above analyses, we may consider the neat $[Cu^I_4L_4]^{4+}$ as a redox-active coordination cage by incorporating multiple $Cu^+$ ions, which are characteristic of inherent redox behaviors. The out-cage catalytic activity of such a coordination cage can be modulated by host–guest interactions. When the host–guest unfit anions, such as $OTs^-$ and $OTf^-$ are applied, the cage shows the lowest solution stability and highest redox activity, undergoing partial dissociation and self-oxidation to yield $Cu^{2+}$ complexes accompanied by the hydroxylation of the ligands[27] (Scheme 3). This accounts for their decreased and non-recyclable out-cage catalytic activity, evidenced by the appearance of various new ESI-TOF MS peaks related to the hydroxylated ligand after the catalytic reaction (Supporting Information Figures S8–9). In the case of small anions such as $ClO_4^-$ and $NO_3^-$, the anion-guested $[Cu^I_4L_4]^{4+}$ cages are formed, endowing them with kinetic and thermodynamic stability while having a relatively low redox activity to remain stable in solution in ambient air. However, the exactly matching $ClO_4^-$ guest deactivates all four $Cu^+$ sites, resulting in the most redox-inactive cage, **3**. Nonetheless, **3** still showed some out-cage catalytic activity comparable with those of **1** and **2** as a result of more chances for a substrate to approach the $Cu^+$ sites, as discussed above. As for cage **4**, the $NO_3^-$ guest elaborately maintains the solution stability and redox activity, leading to robust out-cage catalytic activity owing to the heterogeneity of four $Cu^+$ sites, of which at least one is always free of interaction and remaining active for out-cage intermolecular reaction. Recovery of cages **3** and **4** after the catalytic reaction is evidenced by almost unchanged ESI-TOF MS profiles, as seen from Supporting Information Figures S5–7, and catalytic contribution from the dissociated species may be unlikely because unstable **1** and **2** give only relatively lower yields.

**3.4. Catalyst Recycling.** To check the robustness of the $Cu^+$ cages as homogeneous catalysts capable of repeating use, the catalyst recycling test has been carried out for tetralin oxidation by **4** using four runs. On completion of each stage, the products were analyzed as usual, and the catalyst was recovered by full evaporation of the reaction mixture under vacuum. The subsequent cycles were initiated upon addition of new standard portions of all other reagents. After repeating the experiment for four times, only a slight yield drop of 3.3% was detected (Figure 5 and Supporting Information Table S9), and the catalytic activity was maintained at almost the original level with a rather high selectivity around 92.5% (Figure 5). Data of


dx.doi.org/10.1021/cs300640r | ACS Catal. 2013, 3, 1–9

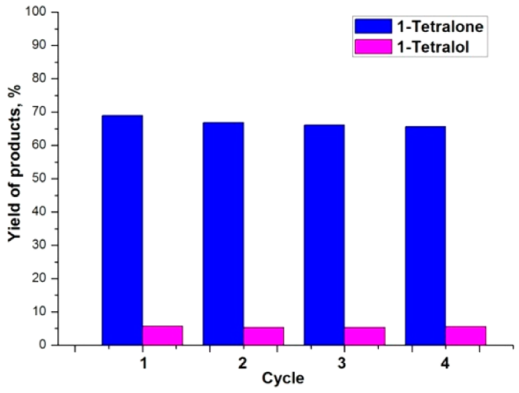


**Figure 5.** Effect of the catalyst recycling on the oxidation of tetralin catalyzed by complex **4**.

both ESI-TOF MS and $^1$H NMR indicate that the $[Cu^I_4L_4]^{4+}$ cage remains in solution after the fourth recycling experiment, with an overall TON larger than 280, shown by observations of the same $^1$H NMR signal profile (Figure 2h) and the neat MS peaks of trivalent $[Cu^I_4L_4(NO_3)]^{3+}$ and divalent $[Cu^I_4L_4(NO_3)_2]^{2+}$ (Supporting Information Figure S6) as those of the original complex **4**. Hence, we can conclude that catalyst **4** is rather stable and recyclable. The slight activity decrease may be related to the corresponding lowering of the catalyst concentration in the reaction mixture as a result of the losses of the samples taken for the GC/MS tests.

**3.5. Mechanism Considerations.** Indirect probes have been used to deduce the reaction mechanism, including radical traps, a regioselectivity study, and the KIE value.

*3.5.1. Effect of Radical Traps.* To determine if the catalytic reaction involves a radical process, several reactions were performed in the presence of various radical trapping agents, such as a carbon-radical trap of TEMPO and an oxygen-radical trap of $Ph_2NH$. The obtained results for the oxidation of tetralin with **4** are listed in Supporting Information Table S10. It is clear that in the presence of both radical traps, formation of 1-tetralone and 1-tetralol products is suppressed and the yield drops to almost zero, indicative of a pronounced catalytic activity decrease of **4**. These observations suggest that both the carbon and oxygen radicals might exist in the oxidation of tetralin with catalyst **4**, in agreement with free radical processes normally reported for the transition-metal-catalyzed oxidation of hydrocarbons in the presence of TBHP using the MeCN solvent.[35−37]

*3.5.2. Regioselectivity Studies.* To investigate the nature of the oxidant, an intramolecular competition reaction in the oxidation of adamantine has been studied (Scheme 4). As an example substrate, adamantine contains both secondary and tertiary C−H bonds and is well-known to show regioselectivity at different C−H bonds. The rigid molecular framework of adamantane makes its hydrogen abstraction from a tertiary position necessarily generate a pyramidalized and destabilized bridgehead radical.[38] Cage **4** was found to be active toward oxidation of adamantane, offering the main product as adamantan-1-ol, whereas the minor products are adamantan-2-ol and adamantan-2-one with a total yield of 29.0% (Supporting Information Table S11). The regioselectivity can be parameterized as a 3°/2° ratio, which is derived from the amount of 1-adamantanol divided by the amounts of 2-adamantanol and 2-adamantanone and multiplied by 3 to correct for the higher number of secondary C−H bonds.[38] As

**Scheme 4. Product Distribution in the Oxidation of Adamantane, Catalyzed by Cage 4**

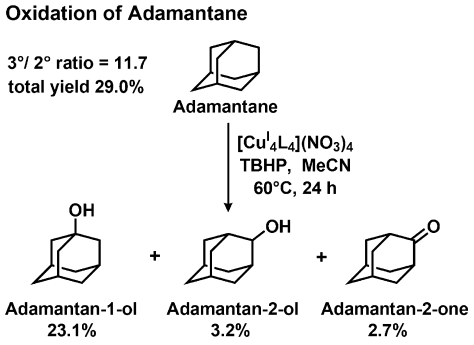


seen from Supporting Information Table S11, a significant 3°/2° ratio of 11.7 for the oxidation of adamantane is achieved, which confirms that the reactivity at the tertiary position is much higher than that at the secondary position. For comparison, HO•-initiated reactions exhibit the 3°/2° selectivity near 2, whereas $^t$BuO• affords values around 10. From the above discussion, it can be concluded that the peroxidative oxidation of alkanes catalyzed by complex **4** cannot be initiated by the indiscriminate HO•.

*3.5.3. KIE Experiments.* The KIE value was evaluated with intermolecular competition experiments by using an equimolar mixture of tetralin and deuterated tetralin as substrates, represented by the reaction with catalyst **4** (Scheme 5). The

**Scheme 5. Deuterium Kinetic Isotope Effects on the Oxidation of Tetralin/Tetralin-$d_4$ (1/1)**

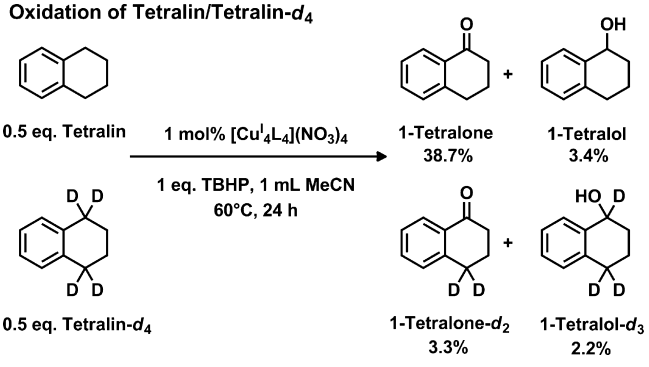


calculation of the KIE value of 7.6 is based on the product distribution of 1-tetralone and 1-tetralol over deuterated 1-terlone and 1-tetralol (Supporting Information Table S12).[39,40] For comparison, the KIE values of the peroxidative oxidations of alkanes in the presence of the oxidants of HO•,[41] $^t$BuO•,[42] P450,[43] and MMO[44] are in the range of 1−2, 4−5, larger than 11, and 50−100, respectively. In the case of P450 and MMO, it is believed that the oxidants are metal-based oxidants. The KIE value of 7.6 is similar to those of the oxidation reactions of cyclohexane and cyclohexane-$d_{12}$ catalyzed by non-heme iron complexes, such as $[Fe_2O(bpy)_4(H_2O)_2](ClO_4)_4$ (KIE = 7.1),[39] $[Fe_2(BPEA)_2O(OAc)](ClO_4)_3$ (7.3),[45] and $[Fe_2O(phen)_4(H_2O)_2](ClO_4)_4$ (7.8).[40] In all of these reactions, TBHP was used as the oxidant. This high KIE value again rules out the possibility of the indiscriminate hydroxyl radical intermediate. On the basis of our current data, unfortunately, it is not yet clear whether the active oxidant is $^t$BuO• only or both $^t$BuO• and the metal-based species, since our KIE value of


dx.doi.org/10.1021/cs300640r | ACS Catal. 2013, 3, 1−9

7.6 is higher than the general KIE values around 5 in $^{t}$BuO•-initiated reactions.

It is noted that in this competition experiment, the total GC yield of 1-terlone and 1-tetralol is around 42.1%, much lower than that of 74.6% (Supporting Information Table S8) in the catalyst screen test under similar reaction conditions. This can be explained by the fact that in the competition experiment (Scheme 5), catalyst **4** is inactive for deuterated tetralin, and as a matter of fact, the mole ratio of tetralin to **4** becomes 50, but not 100 in the catalyst screen test. The yield of 42.1% is consistent with the data (50.6%, entry 5) shown in Supporting Information Table S5 displaying the effect of the tetralin-to-**4** molar ratio.

*3.5.4. Hypothesis of Mechanism.* From the above discussion, we see that the $[Cu^{I}_{4}L_{4}]^{4+}$ cages can efficiently promote intermolecular oxidation of hydrocarbons in a homogeneous catalytic way under mild conditions. The KIE value of 7.6 and 3°/2° selectivity of 11.7 suggests that the oxidation reactions might involve the $^{t}$BuO• radical intermediate. Therefore, a possible oxidation route might be envisaged on the basis of equations proposed by Kochi, as shown in Scheme 6.[46−48]

**Scheme 6. Possible Metal-Based Oxidation Processes Involving TBHP**[a]

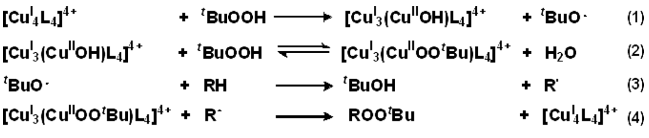


[a] $Cu^{+}/Cu^{2+}$ reactive centers on the cage are arbitrarily represented.

From single-crystal structural analysis, we know that the trigonally coordinated $Cu^{+}$ ion is coordinatively unsaturated and spacious for TBHP to apprach from outside the cage, thereby being activated.[34] However, if the $Cu^{+}$ site interacted with the guest anion to form a weak Cu···O bond, the 3-coordinated $Cu^{+}$ became 4-coordinated pseudotetrahedral $Cu^{+}$, which was likely to be less active. As depicted in Scheme 6, the first step of the catalytic reactions is the reduction of $^{t}$BuOOH by the $Cu^{+}$ ion, in which the trigonal $Cu^{+}$-reactive center might be transformed into triangular pyramidal copper-based oxidant intermediates simplified as $[Cu^{II}{-}OH]^{+}$, while the tetrahedral $Cu^{+}$ center is transformed into trigonal bipyramidal analogs. Meanwhile, the radicals $^{t}$BuO• are generated (eq 1).

Second, the reversible reaction of $[Cu^{II}{-}OH]^{+}$ with $^{t}$BuOOH gives $[Cu^{II}OO^{t}Bu]^{+}$, which remains the same coordination geometry as $[Cu^{II}{-}OH]^{+}$ (eq 2). In both steps, all the $Cu^{+}$ and $Cu^{2+}$ ions are involved in the permitted coordination geometries, which can be interconverted without Cu−N bonds breaking and violent conformation rearranging, going through the formation of intermediate $[Cu^{I}_{4-n}Cu^{II}_{n}L_{4}]^{(4+n)+}$ ($n$ is the number of reactive $Cu^{+}$ centers that are actually involved in catalysis) that can retain the similar cage structure as original $[Cu^{I}_{4}L_{4}]^{4+}$.

The third step is the hydrogen abstraction from hydrocarbons, in which the chain transfer reaction between radical intermediate $^{t}$BuO• and hydrogen donor substrate (RH) will generate alkyl radicals R• (eq 3). In the final step, from the redox of $[Cu^{II}OO^{t}Bu]^{+}$ and alkyl radical R•, intermediate $ROO^{t}Bu$ is accomplished and intermediate $[Cu^{I}_{4-n}Cu^{II}_{n}L_{4}]^{(4+n)+}$ could be quickly reduced to original $[Cu^{I}_{4}L_{4}]^{4+}$, thus achieving one catalytic cycle (eq 4). The alcohol and ketone products could be produced either by the reaction of alkyl radical R• and $O_2$[40,42,45] or from the decomposition of the intermediate $ROO^{t}Bu$.[47]

The trick that $[Cu^{I}_{4}L_{4}]^{4+}$ cage presents a good structural model for supramolecular catalysis for such intermolecular hydrocarbon oxidation may rely on the fact that the out-cage catalytic reactions can proceed effectively through a facilely reversible structural reorganization and host−guest modulation. That is, the coordination changes of $Cu^{+}/Cu^{2+}$ active centers along the catalytic reaction cycle $[Cu^{I}_{4}L_{4}]^{4+} \rightarrow [Cu^{I}_{4-n}Cu^{II}_{n}L_{4}]^{(4+n)+} \rightarrow [Cu^{I}_{4}L_{4}]^{4+}$, from the trigonal $Cu^{+}$ to intermediate triangular pyramidal $[Cu^{II}{-}OH]^{+}/[Cu^{II}OO^{t}Bu]^{+}$ or from tetrahedral $Cu^{+}$ to intermediate trigonal bipyramidal $[Cu^{II}{-}OH]^{+}/[Cu^{II}OO^{t}Bu]^{+}$ are all structurally reversible without destroying the cage integrity. The better activity exerted by cage **4** than cage **3** can be attributed to the more efficient trigonal → triangular pyramidal → trigonal coordination reorganization of the guest non-interacted $Cu^{+}$ centers in **3** during the catalysis process, whereas in **4**, all reactive $Cu^{+}$ centers have to undergo a less effective tetrahedral → trigonal bipyramidal → tetrahedral process. This also demonstrates how the host−guest modulation can affect the catalytic behavior of the cage catalysts.

## 4. CONCLUSION

In summary, we propose an unprecedented supramolecular catalysis structural model by design of nanosized coordination cages installing multiple coordination unsaturated and redox active $Cu^{+}$ sites onto the cage vertices, which facilitates out-cage catalytic reactions and host−guest modulation by judicious selection of guest anions. The solution stability, redox activity and catalytic activity of the cages can be modulated by host−guest interactions on the basis of the size and shape of the cage cavity and anion guest. The preliminary catalysis and mechanism studies reveal that the $NO_3^{-}$ guest-templated $[Cu^{I}_{4}L_{4}]^{4+}$ cage represents the efficient and recyclable catalytic model for oxidation of hydrocarbons via a free radical process, paving the way for applying such coordination cages for a variety of catalytic purposes. Investigations on the use of these cage catalysts for other potential catalytic reactions are in progress.

## ■ ASSOCIATED CONTENT

### Supporting Information

Optimization of catalytic reaction conditions; ESI-TOF mass spectra; Characterization of complexes; CIF files giving crystallographic data. CCDC reference numbers 864852 and 901630. This material is available free of charge via the Internet at http://pubs.acs.org.

## ■ AUTHOR INFORMATION

### Corresponding Author

*E-mails: (L.Z.) zhli99@mail.sysu.edu.cn; (C.-Y.S.) cesscy@mail.sysu.edu.cn.

### Notes

The authors declare no competing financial interest.

## ■ ACKNOWLEDGMENTS

Dedicated to Professor Dieter Fenske on the occasion of his 70th birthday. This work was supported by the 973 Program (2012CB821701) and NSF Projects (21102186, 21121061,

21173272, and U0934003) of China and the Fundamental Research Funds for the Central Universities.

## REFERENCES

(1) Yoshizawa, M.; Klosterman, J. K.; Fujita, M. *Angew. Chem., Int. Ed.* **2009**, *48*, 3418−3438.
(2) Seidel, S. R.; Stang, P. J. *Acc. Chem. Res.* **2002**, *35*, 972−983.
(3) Leininger, S.; Olenyuk, B.; Stang, P. J. *Chem. Rev.* **2000**, *100*, 853−908.
(4) Wiester, M. J.; Ulmann, P. A.; Mirkin, C. A. *Angew. Chem., Int. Ed.* **2011**, *50*, 114−137.
(5) Fiedler, D.; Leung, D. H.; Bergman, R. G.; Raymond, K. N. *Acc. Chem. Res.* **2005**, *38*, 351−360.
(6) Ikemi, M.; Kikuchi, T.; Matsumura, S.; Shiba, K.; Satoa, S.; Fujita, M. *Chem. Sci.* **2010**, *1*, 68−71.
(7) Glasson, C. R. K.; Clegg, J. K.; McMurtrie, J. C.; Meehan, G. V.; Lindoy, L. F.; Motti, C. A.; Moubaraki, B.; Murray, K. S.; Cashion, J. D. *Chem. Sci* **2011**, *2*, 540−543.
(8) Turega, S.; Whitehead, M.; Hall, B. R.; Haddow, M. F.; Hunter, C. A.; Ward, M. D. *Chem. Commun.* **2012**, *48*, 2752−2754.
(9) Saalfrank, R. W.; Maid, H.; Scheurer, A. *Angew. Chem., Int. Ed.* **2008**, *47*, 8794−8824.
(10) Tan, G.; Yang, Y.; Chu, C.; Zhu, H.; Roesky, H. W. *J. Am. Chem. Soc.* **2010**, *132*, 12231−12233.
(11) Kilbas, B.; Mirtschin, S.; Scopelliti, R.; Severin, K. *Chem. Sci.* **2012**, *3*, 701−704.
(12) Weckhuysen, B. M. *Angew. Chem., Int. Ed.* **2009**, *48*, 4910−4943.
(13) Leung, D. H.; Fiedler, D.; Bergman, R. G.; Raymond, K. N. *Angew. Chem., Int. Ed.* **2004**, *43*, 963−966.
(14) Leung, D. H.; Bergman, R. G.; Raymond, K. N. *J. Am. Chem. Soc.* **2007**, *129*, 2746−2747.
(15) Yoshizawa, M.; Tamura, M.; Fujita, M. *Science* **2006**, *312*, 251−254.
(16) Smulders, M. M. J.; Nitschke, J. R. *Chem. Sci.* **2012**, *3*, 785−788.
(17) Nishioka, Y.; Yamaguchi, T.; Yoshizawa, M.; Fujita, M. *J. Am. Chem. Soc.* **2007**, *129*, 7000−7001.
(18) Merlau, M. L.; Mejia, M. d. P.; Nguyen, S. T.; Hupp, J. T. *Angew. Chem., Int. Ed.* **2001**, *40*, 4239−4242.
(19) Yoon, H. J.; Mirkin, C. A. *J. Am. Chem. Soc.* **2008**, *130*, 11590−11591.
(20) Noh, T. H.; Heo, E.; Park, K. H.; Jung, O. S. *J. Am. Chem. Soc.* **2011**, *133*, 1236−1239.
(21) Amouri, H.; Desmarets, C.; Moussa, J. *Chem. Rev.* **2012**, *112*, 2015−2041.
(22) Hastings, C. J.; Backlund, M. P.; Bergman, R. G.; Raymond, K. N. *Angew. Chem., Int. Ed.* **2011**, *50*, 10570−10573.
(23) Phipps, R. J.; Gaunt, M. J. *Science* **2009**, *323*, 1593−1597.
(24) Peterson, R. L.; Himes, R. A.; Kotani, H.; Suenobu, T.; Tian, L.; Siegler, M. A.; Solomon, E. I.; Fukuzumi, S.; Karlin, K. D. *J. Am. Chem. Soc.* **2011**, *133*, 1702−1705.
(25) Matsumoto, T.; Ohkubo, K.; Honda, K.; Yazawa, A.; Furutachi, H.; Fujinami, S.; Fukuzumi, S.; Suzuki, M. *J. Am. Chem. Soc.* **2009**, *131*, 9258−9267.
(26) Harmata, M. *Silver in Organic Chemistry*; John Wiley & Sons, Inc.: Hoboken, NJ, 2010.
(27) He, Q.-T.; Li, X.-P.; Liu, Y.; Yu, Z.-Q.; Wang, W.; Su, C.-Y. *Angew. Chem., Int. Ed.* **2009**, *48*, 6156−6159.
(28) Su, C.-Y.; Cai, Y.-P.; Chen, C.-L.; Smith, M. D.; Kaim, W.; Loye, H. C. z. *J. Am. Chem. Soc.* **2003**, *125*, 8595−8613.
(29) Su, C.-Y.; Cai, Y.-P.; Chen, C.-L.; Lissner, F.; Kang, B.-S.; Kaim, W. *Angew. Chem., Int. Ed.* **2002**, *41*, 3371−3373.
(30) Sheldrick, G. M. In *SHELX 97; program for crystal structure solution and refinement*; University of Göttingen: Göttingen, Germany, 1997.
(31) *CrysAlis RED*, Version 1.171.31.7; Oxford Diffraction Ltd.: Abington, England, 2006.
(32) Greenwald, R.; Chaykovsky, M.; Corey, E. J. *J. Org. Chem.* **1963**, *28*, 1128−1129.
(33) Comlta, P. B.; Berman, M. R.; Moore, C. B.; Bergman, R. G. *J. Phys. Chem.* **1981**, *85*, 3266−3276.
(34) Kirillov, A. M.; Kopylovich, M. N.; Kirillova, M. V.; Haukka, M.; Silva, M. F. C. G. d.; Pombeiro, A. J. L. *Angew. Chem., Int. Ed.* **2005**, *44*, 4345−4349.
(35) Barton, D. H. R.; Hu, B.; Taylor, D. K.; Wahl, R. U. R. *J. Chem. Soc., Perkin Trans. 2* **1996**, 1031−1041.
(36) Barton, D. H. R.; Beck, A. H.; Taylor, D. K. *Tetrahedron* **1995**, *51*, 5245−5254.
(37) Barton, D. H. R.; Taylor, D. K. *Pure Appl. Chem.* **1996**, *68*, 497−504.
(38) Costas, M.; Chen, K.; Que, L., Jr. *Coord. Chem. Rev.* **2000**, *200*−*202*, 517−544.
(39) Ménage, S.; Vincent, J. M.; Lambeaux, C.; Chottard, G.; Grand, A.; Fontecave, M. *Inorg. Chem.* **1993**, *32*, 4766−4773.
(40) Ménage, S.; Vincent, J. M.; Lambeaux, C.; Fontecave, M. *J. Mol. Catal. A: Chem.* **1996**, *113*, 61−75.
(41) Buxton, G. V; Greenstock, C. L.; Helman, W. P.; Ross, A. B. *J. Phys. Chem. Ref. Data* **1988**, *17*, 513−886.
(42) MacFaul, P. A.; Ingold, K. U.; Wayner, D. D. M.; Que, L., Jr. *J. Am. Chem. Soc.* **1997**, *119*, 10594−10598.
(43) Sono, M.; Roach, M. P.; Coulter, E. D.; Dawson, J. H. *Chem. Rev.* **1996**, *96*, 2841−2887.
(44) Nesheim, J. C.; Lipscomb, J. D. *Biochemistry* **1996**, *35*, 10240−10247.
(45) Leising, R. A.; Kim, J.; Pérez, M. A.; Que, L., Jr. *J. Am. Chem. Soc.* **1993**, *115*, 9524−9530.
(46) Kochi, J. K. *Tetrahedron* **1962**, *18*, 483−497.
(47) Feldberg, L.; Sasson, Y. *Tetrahedron Lett.* **1996**, *37*, 2063−2066.
(48) Gillner, D.; Zawadiak, J.; Mazurkiewicz, R.; Kurczewska, J.; Schroeder, G.; Orlińska, B. *Monatsh. Chem.* **2010**, *141*, 143−147.